Synchronization of Low Voltage Grids Fed by Smart and Conventional Transformers

Stefano Giacomuzzi, Giovanni De Carne, *Member, IEEE,* Sante Pugliese, *Member, IEEE,* Giuseppe Buja, *Life Fellow, IEEE* Marco Liserre, *Fellow, IEEE* and Ali Kazerooni

Abstract—The Smart Transformer (ST) is a power electronics-based transformer, which operates as grid-forming converter in the low voltage-fed grid. It synthesizes the voltage waveform with magnitude, phase and frequency independently from the main power system. If a meshed operation of the ST with a conventional transformer is required, to improve the power flow control and to control the voltage profile, the voltage waveforms between the two grids have to be synchronized. The switching under different voltage magnitude, phase or frequency, can lead to a large power in-rush. This work proposes a synchronization strategy that enables a seamless transition of the ST to parallel operations with conventional transformers. Differently from classical communication-based methods, this work addresses a more realistic implementation case with limited communication infrastructure. The ST relies only on local measurements and on its advanced control capability to determine the effective switch to parallel operations. The performance of the proposed strategy has been proved analytically and through simulations in a PLECS/Matlab environment, and validated experimentally by means of Power-Hardware-In-Loop (PHIL) evaluation.

Index Terms—Smart Transformer, Solid State Transformer, Power Hardware In the Loop, Normally Open Point.

I. Introduction

THE spread of distributed generation challenges the distribution grid operations, particularly the voltage control. An uncontrolled power injection affects the voltage amplitude, that can reach the over- or under limits. In unusually critical conditions, the distribution system operator can reconfigure the grid by connecting the loads to another feeder by closing the Normally Open Point (NOP) switch. This action changes the power flow in the grid, and thus its voltage profile. However, the synchronization between two grid is not straightforward, since their respective voltages are initially non-synchronized, with different voltage amplitude and phase, and, eventually,

S. Giacomuzzi and G. Buja are with the Department of Industrial Engineering, University of Padova, Padova 35122, Italy (e-mail: stefano.giacomuzzi@phd.unipd.it; giuseppe.buja@unipd.it).

G. De Carne is with the Institute for Technical Physics, Karlsruhe Institute of Technology, 76344 Karlsruhe, Germany (e-mail: giovanni.carne@kit.edu).

S. Pugliese and M. Liserre are with the Chair of Power Electronics, Kiel University, 24143 Kiel, Germany (e-mail: sapu@tf.uni-kiel.de; ml@tf.uni-kiel.de).

A. Kazerooni is with the SP Energy Networks, Glasgow, UK (e-mail: akazerooni@spenergynetworks.co.uk). The work has been conducted in collaboration with SP Energy Networks as part of LV Engine project which is funded by Ofgem through Network Innovation Competition mechanism.

Giovanni De Carne is supported by the Helmholtz Association under the joint initiative Energy System Design in the Research Field Energy.

Sante Pugliese and Marco Liserre are supported by European Research Council under the European Union's Seventh Framework Programme (FP/2007-2013)/ERC Grant Agreement n. [616344] - HEART.

frequency: an uncontrolled synchronization can lead to large power flow in-rush in the connecting line [1]. Specifically, in this paper the focus is on the synchronization process between one low voltage (LV) grid fed by a conventional transformer and one by a Smart Transformer (ST). The ST, a medium voltage (MV)/LV power electronics-based transformer, is considered as one of the most promising technologies to facilitate the integration of renewable sources and electric vehicles in the grid. Its advanced controllers enable the provision of grid services, that go beyond the simple voltage level transformation [2]–[5].

The synchronization problem between power electronics-devices with the grid can be found in the microgrid reconnection with the mains after islanding [6]. However, in microgrids several energy sources contribute to support the grid according to their power rating. Most of the power converters work in grid-forming mode, providing voltage and frequency stability, but they are usually supported by converters that work in grid-following mode, usually fed by non-programmable sources. In case of abrupt reconnection, the microgrid can still be supported by the main grid, which is often considered as a stiff grid. On the opposite, in the case of ST-fed and conventional transformer-fed grids, the ST is in charge to supply its own loads before the closure of the NOP, that are comparable to the conventional transformer ones. In case of abrupt connection, the ST can overload, and the grid-forming converter shuts down. As a consequence, the conventional transformer has to provide power to the loads of two grids, leading to its overload and following shut down. A further issue is represented by considering a fast communication infrastructure, that is a possibility for microgrids in the next years [7], but it is not available in the current distribution network. Instead, the ST technology can be ready as soon as in the next couple of years, as planned by the OFGEM-funded project "LV-ENGINE" [8], where 6 STs will be integrated in the Scottish grid by 2020.

Under these assumption, a seamless transition strategy is vital for safe and reliable operation of Smart and conventional transformers. This paper introduces a control strategy for a smooth synchronization of a ST-fed with a conventional transformer-fed LV grid, that relies on slow communication, on local measurements and local angle synchronization (Fig.1).

In this work, the following novel contributions to the state of the art are introduced:
- Seamless transition between ST- and conventional transformer-fed LV grids, comparable in power.
- The proposed approach relies only on local measurements and local angle synchronization.

TABLE I
STATE OF THE ART OF SEAMLESS TRANSITION

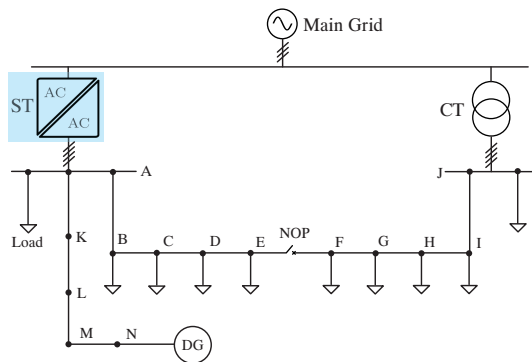| Feature \ Reference	[9], [10]	[11]	[12]–[14]	[7], [15], [16]	[17]–[19]	[20]–[22]	[23]	[24]	[25]	[26]	Proposed strategy
Grid forming	✓	✓	✓	✓	✓	✓	✓	✗	✓	✓	✓
Only slow communication	✗	✓	✗	✗	✗	✓	✓	✓	✗	✓	✓
Generic placement in the grid	✓	✓	✗	✓	✓	✗	✗	✗	✗	✗	✓
Local current & voltage meas.	✓	✓	✓	✓	✓	✓	✓	✓	✓	✓	✓
Local synchronization	✗	✗	✗	✗	✗	✓	✓	✗	✗	✓	✓
Parameter variation analysis	✗	✓	✗	✗	✓	✗	✓	✓	✓	✓	✓
Islanded to grid-connected	✗	✗	✓	✓	✓	✓	✓	✗	✓	✓	✓

Fig. 1. Schematic of the analyzed two-feeder radial distribution grid.

- Only slow communication, that already exists in distribution grids, is considered.
- The effectiveness of proposed strategy has been validated through PHIL experimental setup.

The paper is organized with Section II that reviews the state of the art of the seamless transition for microgrids and briefly introduces the characteristics of ST. Section III investigates the impact of voltage phase and magnitude difference on the steady-state power flow, after the NOP closure. Section IV presents the proposed synchronization strategy for the ST, which is then validated in Section V through simulation in PLECS/Matlab environment for three significant cases. Section VI is dedicated to confirm the findings through Power-Hardware-in-the-Loop (PHIL) based experimental results. Section VII concludes the paper.

Throughout the paper, upper-case letters denote pu quantities, to differentiate from the time-variable ones which are represented in lower-case letters.

II. STATE OF THE ART

A. Seamless transition

As mentioned in the introduction, the seamless transition topic has been deeply examined in recent literature, particularly regarding the microgrid reconnection with the main grid. Nonetheless, some existing works focus on the transition from grid-connected to islanded mode, without investigating

the reverse transition to the main grid connection [9]–[11], which is the aim of this paper.

In microgrids, the communication infrastructure technology is often utilized, making the measurement of voltage angle and magnitude available for any converter in the grid. The availability of such measurements facilitates the synchronization process, which can be integrated in the secondary control of hierarchical control structures [7], [13], [15], [16], [25]. In [14] the mains voltage is measured and communicated to the synchronizing converter, that uses a Phase-Locked-Loop (PLL) to obtain the magnitude and angle. The need for PLL is overcome in [12] with the introduction of an integrated synchronization and control technique, which still requires the mains voltage measurements through a low-bandwidth communication link. The same occurs in [19], with the required signals that is transmitted to the centralized control system and then sent back to the switch and to the inverters primary controls. In [17] a fiber cable is installed between the switch and the converter acting as a master for the microgrid, while in [18] an Ethernet network ensures a fast communication.

Synchronization strategies without the need for a communication link, require still the mains voltage measurement. For instance, in [20] there is a unit in charge of the resynchronization, which is placed close to the switch. Thus the voltage measurement is taken as reference. Reference [21] presents an indirect current control algorithm for seamless transition of three-phase inverters. The idea is to regulate the grid-side inductor current by controlling the magnitude and phase angle of the voltage across the filter capacitor. The circuit adopted involves a critical load placed in proximity to the inverter, and immediately after there is the switch for the grid connection. In this approach, the grid reconnection procedure is facilitated by the availability of the grid voltage measurement. The authors in [22] present and compare different techniques to match the grid and the inverter angle, but all of them require the grid voltage measurement. In [23] the pre-synchronization is used to synchronize the voltage and frequency of the microgrid and the main grid using PLL technique. It is implemented in the master inverter, which is placed close to the reconnection switch so as the grid voltage measurements are easily available. The concept of PLL-less operation of grid-connected converters has been recovered in [24]. Here, the authors introduce the

inducverters, that are so called for their dynamics similar to the induction machines with soft-synchronization capabilities; as disadvantage, they are conceived only as grid-following converters. A method for seamless transition of three-phase inverters is proposed in [26], which allows them to respond very quickly if the grid and the PCC voltages are out of phase. The inverter current is greater than $2\ pu$ for $1/38$ of a cycle. After this overcurrent, the inverter enters in coast mode, i.e. it turns off all the IGBTs for half a cycle. This would represent an issue for the ST that, as mentioned in the introduction, feeds the whole LV grid loads.

As per the state of the art, the situation discussed in this paper has never been found in literature. Either the proximity to the switch or the communication link make the voltage measurement in some way available for the converter in charge of the synchronization process. Table I summarizes the main points for several of the most significant works on the synchronization. The classification has been performed by dividing these works by their grid-forming characteristics, and by two factors that facilitates the synchronization with the main grid, i.e. the presence or less of fast Information and Communication Technology (ICT) and the generic placement of the NOP in the grid.

B. The Smart Transformer Concept

The ST is a solid-state transformer, interfacing MV and LV distribution grids, able to provide services to the distribution grids. Although different architectures are possible [27], the three-stage configuration can provide more functionalities compared to other designs, as for example the LV Direct Current (DC) and MV DC connections for renewables and electric vehicle integration. In a three-stage design, the ST MV converter regulates the MV DC-link voltage through active power absorption from MV grid and controls the reactive power injection [28]. The DC/DC converter, in addition to providing galvanic isolation with a high frequency transformer, regulates the power flow between MV and LV DC-links to regulate the LV DC-link voltage. Regarding the LV converter, two working modes are possible (Fig.2a): i) grid-forming mode, that synthesizes the grid voltage waveform, with the current that is determined by the load demand; ii) grid-following mode, that follows the grid voltage, to regulate the active and reactive current injection in the LV grid.

This work focuses on the transient period during the synchronization procedure, when the ST LV converter remains in grid-forming mode (see top half of Fig.2b), before switching to the power control in grid-following mode. Two signals are delivered by the NOP to ST: the first, denoted as NOP closure signal, states the NOP closure request and, therefore, to start the closing procedure. The second, indicated as NOP effective closure signal, determines that NOP has been effectively closed; only after receiving this signal, ST shifts to the grid-following mode, as shown in blue boxes in Fig.2b. However, the communication signals can reach the ST after tens of seconds, if not minutes, after the NOP closure, due to the slow bandwidth of the current communication infrastructure. For this reason, i) after sending out the closure signal, the NOP
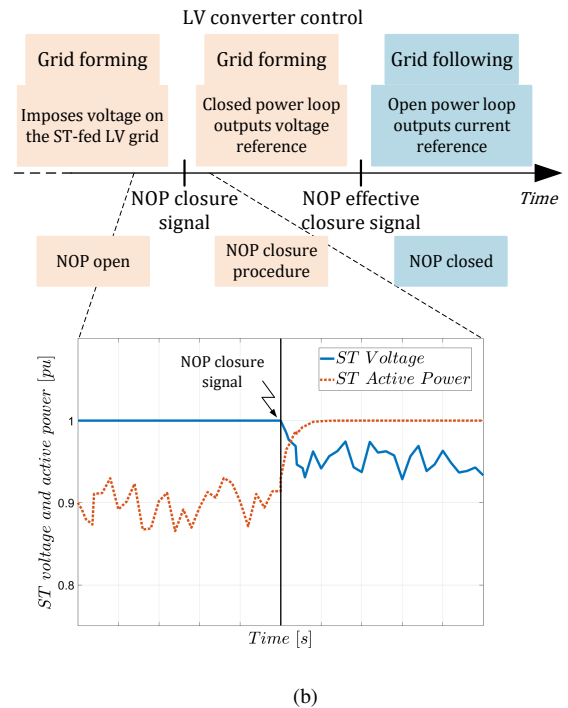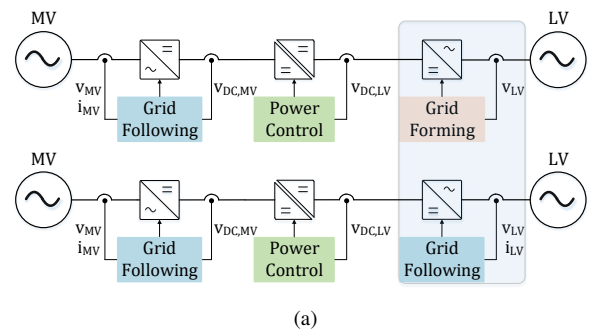

Fig. 2. (a) Three-stages Smart Transformer with relevant control tasks for each stage, (b) LV converter control under different NOP conditions and qualitative effects of ST control on voltage (solid blue line) and power (dotted red line) profile.

has to wait for a sufficient time that the signal is received by the ST, before effectively starting the closure procedure; ii) the ST control needs to detect the effective NOP closure only from its output measurements.

When it receives the NOP closure signal, the ST remains in grid-forming mode. An external control loop is activated to control the power injection in the LV grid, varying the voltage magnitude. This feature ensures that the active power injected by ST remains constant during the operation. During this period, any power changes, caused by loads and generators, are handled by this external voltage/power controller. It has been assumed that large power variations are not present during this time window (few minutes at most), and, if they occur, the voltage controller is able to address them (see study case in Section V.B). The lower part of Fig.2b shows a qualitative behavior of the ST LV converter, when it switches from the voltage control in grid-forming mode to the power control varying actively the voltage. It is worth noting that the controls are enabled by low bandwidth signals delivered by the NOP,

TABLE II
BASE VALUES AND LOAD POWER OF THE CASE STUDY

Parameter	Base Value		Node	Active Power [p.u.]
Base Voltage	400 V		A, J	0.67
			B, C, D, E	0.05
Base Power	300 kVA		F, G, H, I	0.083
			N	−0.083

TABLE III
LINE IMPEDANCE OF THE CASE STUDY

Busbar		Resistance [p.u.]	Reactance [p.u.]
A-B, B-C, H-I, I-J		0.0263	0.0119
C-D, D-E, E-F, F-G, G-H		0.0404	0.0121
A-K		0.0527	0.0239
K-L, L-M		0.0808	0.0242
M-N		0.0963	0.00257

and no fast communication is implemented in this application.

III. ANALYSIS OF POWER TRANSFER IN MESHED OPERATIONS

This section aims to analyze the power flow during the synchronization of the ST with the transformer-fed grid under different voltage magnitude and angle. The analysis is performed considering a typical UK two feeder radial distribution grid, shown in Fig.1. It is assumed that the ST and the conventional transformer are fed by the same MV grid and they both operate as grid-forming for the LV-fed grids. The adopted base values are pointed out in Table II, together with the loads active power: the nominal voltage in LV European lines has been selected as base voltage, whilst the base power is the rated power of ST. The power factor is set at 0.95 for all the loads. The Distributed Generation (DG) unit is controlled to inject only active power (denoted with negative sign). Table III expresses the pu line impedances.

As well known in literature, the line resistance in transmission line is commonly neglected. However, if LV lines are considered, both resistive and inductive components need to be both taken into account, since the X/R ratio is lower than unity. Following this assumption, the pu complex power delivered by ST can be calculated as:

$$P_{ST} + jQ_{ST} = V_{ST}\angle\theta_{ST}\left(I_{ST}\angle\theta_{I,ST}\right)^* =$$
$$= V_{ST}\angle\theta_{ST}\left(\frac{V_{ST}\angle\theta_{ST} - V_{CT}\angle\theta_{CT}}{R_{eq} + jX_{eq}}\right)^* \quad (1)$$

where P_{ST} and Q_{ST} are ST output active and reactive power, respectively, V_{ST}, I_{ST}, V_{CT}, θ_{ST}, $\theta_{I,ST}$ and θ_{CT} are the ST output voltage and current rms values, the conventional transformer output rms voltage, the ST voltage and current angle and the conventional transformer voltage angle, respectively; R_{eq} and X_{eq} are the equivalent resistance and reactance between the ST and the transformer, respectively, if the NOP is closed; the superscript * denotes complex conjugate quantity. After some manipulations of (1) and splitting real and imaginary part, the active and reactive power delivered by ST can be represented by (2) and (3), respectively:

$$P_{ST} = \frac{V_{ST}}{Z_{eq}^2}\left[R_{eq}\left(V_{ST} - V_{CT}\cos\theta_{CT}\right) - V_{CT}X_{eq}\sin\theta_{CT}\right] \quad (2)$$

$$Q_{ST} = \frac{V_{ST}}{Z_{eq}^2}\left[X_{eq}\left(V_{ST} - V_{CT}\cos\theta_{CT}\right) + V_{CT}R_{eq}\sin\theta_{CT}\right] \quad (3)$$
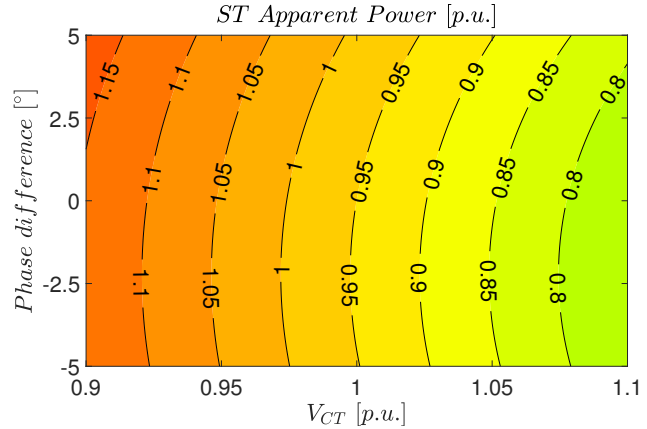

Fig. 3. Apparent power delivered by ST expressed in p.u. as a function of conventional transformer voltage and angle.

The phase angle θ_{ST} is chosen as reference and set at $0°$. In Fig.3 the ST apparent power is plotted as a function of v_{CT} magnitude and phase. The figure has been obtained adopting the superposition principle, short-circuiting before the ST and subsequently the conventional transformer and then summing output current of the ST in the two situations. The ST has been considered working with voltage magnitude V_{ST} and phase θ_{ST} at 1.025 pu and $0°$, respectively. As already expressed in (2) and (3), since R_{eq} is higher than X_{eq}, the voltage magnitude affects mainly the active power, while the reactive power depends on the phase angle difference. During synchronization, it is important to avoid the conditions that lead to the ST overload. As can be noted in Fig.3, the worst situation for the ST is during undervoltage conditions of the transformer-fed LV grid. Indeed, after the NOP closure, the ST overloads. Under these conditions, the transformer phase angle does not influence appreciably the ST power, due to the smaller contribution from reactive power in comparison of the active power. As an example, if we consider $V_{CT} = 0.95$ pu and $\theta_{CT} = 2°$, the steady-state ST active power becomes 0.97 pu and reactive power 0.37 pu. As a consequence, the apparent power delivered by ST is 1.04 pu, with a resultant overload. It can be concluded that the voltage difference between the ST and the conventional transformer has to be strictly controlled in order to avoid the ST overload.

IV. CONTROL STRATEGY OF THE ST

This section proposes a synchronization strategy to control the power flow of STs in case of slow communication infrastructure. The following assumptions have been made:
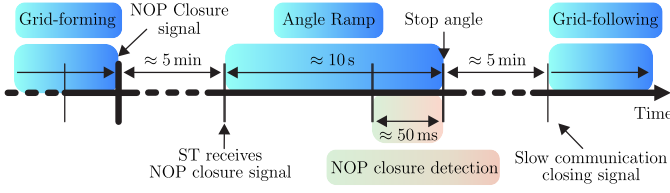
Fig. 4. Timeline of the NOP closure procedure.

a) Only low bandwidth industrial communication is established between the NOP and ST (e.g., SCADA); signals transfer may range in tens of seconds, if not minutes.
b) The NOP can close within a certain phase difference $\Delta\theta_{\text{NOP}}$ (i.e., $\pm 2°$) at its extremities, and it is rated large enough to withstand the in-rush current during its closure.
c) The ST LV converter works in grid-forming mode with magnitude higher than the transformer (i.e., $V_{\text{ST}} = 1.025$ pu) and phase $\theta_{\text{ST}} = 0°$ prior to the NOP closure signal.

An uncoordinated synchronization between the two LV feeders can cause large current inflow, created by the difference in voltage amplitude and phase between the two voltage sources (i.e., ST and transformer). In order to limit this current, and therefore the exchange of active and reactive power between the two voltage sources, the difference in frequency, phase angle and magnitude of the voltage at NOP extremities should be minimized. Concerning the frequency, this work considers the case where the ST and transformer feeders are connected to the same MV grid, sharing the same frequency. It has been assumed in this work that the ST works at nominal frequency (i.e., 50 Hz). As a consequence, only phase angle and magnitude differences of the voltage still need to be addressed.

The timeline of the proposed safe NOP switching strategy for ST is shown in Fig.4. Once the distributor system operator establishes the NOP closure, the NOP sends a signal to ST (it may require several minutes due to the slow communication), communicating the closure request. Then, the NOP switching strategy is composed of three stages:

(i) ST controls the active power varying the output voltage magnitude;
(ii) ST varies its output voltage angle, to match the transformer angle;
(iii) ST detects the NOP closure measuring its output reactive power.

As shown in Fig.5, stages (i) and (ii) contribute to generate the voltage reference for ST, while stage (iii) is important to detect the NOP closure and halt the progress of stage (ii). After receiving the effective closure signal from NOP, ST finally can shift to the grid-following mode, synchronizing to the voltage imposed by the conventional transformer.

A. ST active power control

The small phase difference at the NOP terminals (condition b)), that guarantees the switch closure, allows us to neglect the voltage phase impact and consider only the effect of V_{CT} on P_{ST} and Q_{ST} variation. As demonstrated in Section III,
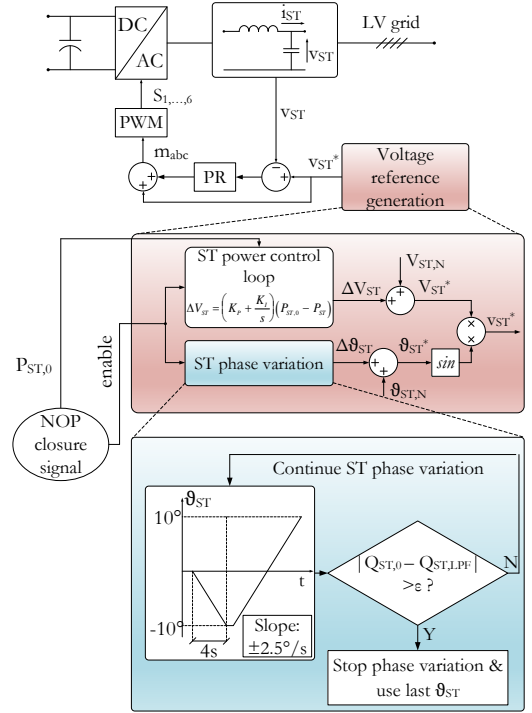

Fig. 5. Control scheme of ST LV converter.

the voltage difference affects the ST active power more than the reactive one; for this reason, in this strategy the generation of the voltage reference amplitude involves the active power. When ST receives the NOP closure signal, it stores the active power measured at its output, denoted as $P_{\text{ST},0}$, in order to preserve the initial power flow after the synchronization. A closed-loop control is implemented with a proportional integral controller, tracking the ST active power at the value $P_{\text{ST},0}$ by controlling the output voltage. The output of the controller is the voltage ΔV_{ST} that is added to nominal voltage set-point $V_{\text{ST,N}}$ to obtain the new voltage reference V_{ST}^*.

B. ST angle voltage variation method

As shown in Fig.3, a difference of few degrees in the phase between the two voltage sources leads to a ST power injection increase up to 5%. In order to meet the closure requirements stated in assumption b), the voltage angle of the ST has to be changed, to reduce the difference with the conventional transformer one. Thanks to the decoupling effect of ST with the MV grid, when NOP is open, the ST output power is not affected by variations of the angle. This feature allows to vary dynamically the ST voltage angle, as an example adopted in this work, with a ramp function with a slope coefficient of $2.5°/s$. The phase variation is limited in this work in the range of $(-10° \div +10°)$, considered as worst case for phase difference between the two feeders. It is worth to note that is possible to extend the range in order to include even larger phase differences, although they are not common; hence, this limitation does not affect the validity of the strategy. In this application, the angle control begins from $0°$ with a negative slope. Once reached the saturation value of $-10°$, it

subsequently increases until $10°$, as depicted in the ST phase variation block of Fig.5. The process requires 12.2 s in the worst hypothesis where the phase difference is around $+10°$. If the requirements to close NOP are not met (e.g., higher phase difference), the ST phase angle is brought back at $0°$.

C. NOP closure detection

Among the assumptions listed at the beginning of the section, the low bandwidth communication between NOP and ST is the one that mostly affects the detection of NOP closure. Therefore, ST has to recognize the NOP closure and stop the phase variation, relying only on its measured quantities. If not halted, the phase variation continues to change the ST reactive power injection. Since an active power loop is implemented to avoid increase in P_{ST}, the closure detection cannot be based on active power variation. Starting from this premise, the detection is based only on ST reactive power measurements. To stop the phase change, the strategy shown in the lower part of Fig.5 is implemented. At first, the reactive power is filtered by a lowpass filter with time constant τ_{LPF}, obtaining $Q_{ST,LPF}$, to filter any stochastic power variation.

$$Q_{ST,LPF} = Q_{ST} \frac{1}{1 + s\tau_{LPF}} \quad (4)$$

The ST detects the NOP closure through the difference between $Q_{ST,LPF}$ and the value of reactive power $Q_{ST,0}$, that has been stored once received the closure signal: if this is larger than a certain threshold ϵ, as shown in (5), the ST recognizes the NOP closure and halts the phase variation; if not, the ST voltage phase variation continues.

$$| Q_{ST,0} - Q_{ST,LPF} | > \epsilon \quad (5)$$

The selection of the parameters τ_{LPF} and ϵ defined in (4) and (5) impacts both on the time response and the robustness of the NOP closure detection. Fig.6 shows the reactive power difference $| Q_{ST,0} - Q_{ST,LPF} |$ as a function of the time for a reactive step equal to 0.07 pu, plotted for different parameters τ_{LPF} and ϵ. The algorithm detecs the NOP closure, if the solid line representing $| Q_{ST,0} - Q_{ST,LPF} |$ crosses the horizontal dashed line representing ϵ. As an example, for $\epsilon = 0.05$ p.u., a slow filter (e.g., $\tau_{LPF} = 0.2$ s) leads to detect the NOP closure after 250 ms, a long time for a safe switch. The choice of a faster filter (e.g., $\tau_{LPF} = 0.1$ s) reduces the detection time to about 100 ms, but it may introduce some noise in the power measurement. At the same time, a lower detection threshold ϵ can compensate this problem (e.g., $\epsilon = 0.02$ p.u.), but it may confuse fast reactive power changes in the grid (e.g., capacitor insertion) with the NOP closure.

To achieve a compromise between detection speed, noise rejection and false detection, in this work the two following values have been adopted:

$$\tau_{LPF} = 0.05 \text{ s} \qquad \epsilon = 0.02 \text{ pu} \quad (6)$$

V. SIMULATION RESULTS

The validity of the proposed synchronization strategy has been verified through simulation in PLECS/Matlab environment. Three test cases have been considered:
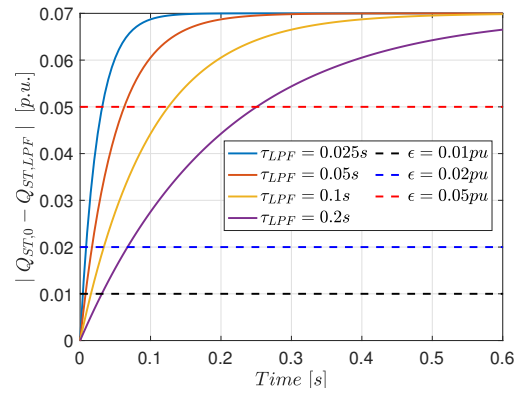

Fig. 6. Time response of NOP closure detection strategy for different time constants τ_{LPF} of the lowpass filter and parameters ϵ.

TABLE IV
PARAMETERS ADOPTED IN THE TEST CASES

Test case	V_{CT} [p.u.]	θ_{CT} [°]	ΔP_{DG} [p.u.]
A	0.95	5	0
B	0.95	5	0.0415
C	1.025	0	0

A) conventional transformer-fed LV grid undervoltage;
B) renewable power variation during closure procedure;
C) synchronization in ideal conditions (zero voltage magnitude and phase difference).

As mentioned, the distribution system operator can request the NOP closure, to support the transformer-fed grid during undervoltage conditions. In the simulation, the ST receives the NOP closure request signal around 3.9 s (see Fig.7a), starting the closure control strategy. Table IV resumes the different values concerning the three cases presented; V_{ST} and θ_{ST} are omitted because are always equal to $V_{ST,N}$ and $\theta_{ST,N}$, respectively.

A. Conventional transformer-fed grid undervoltage

In the first test case, the transformer-fed grid voltage is $V_{CT} = 0.95$ pu and θ_{CT} is equal to $5°$ as initial condition. Note that without the ST phase control, the NOP could not close due to a phase difference at its extremities, that is higher the allowed value ($\pm 2°$). The ST voltage phase and NOP phase difference at NOP extremities during the phase variation are depicted in Fig.7a. If only the voltage phase variation method is implemented, the NOP is able to close, but the difference in voltage magnitude induces an active power flow from the source with higher voltage to the lower one, i.e. from the ST to the conventional transformer. The change in active and reactive power in this case are plotted in the top half of Fig.7b. The simulation results confirm the outcomes of Fig.3: ST active power rises to 0.97 pu, and so does the reactive power from 0.27 pu to 0.37 pu; together they overload ST, with the apparent power reaching 1.04 pu.

Enabling the proposed synchronization strategy, the active power is kept fixed at the value that ST was delivering before the NOP closure signal, as shown by red line in the second subplot of Fig.7b, after a short overshoot transient
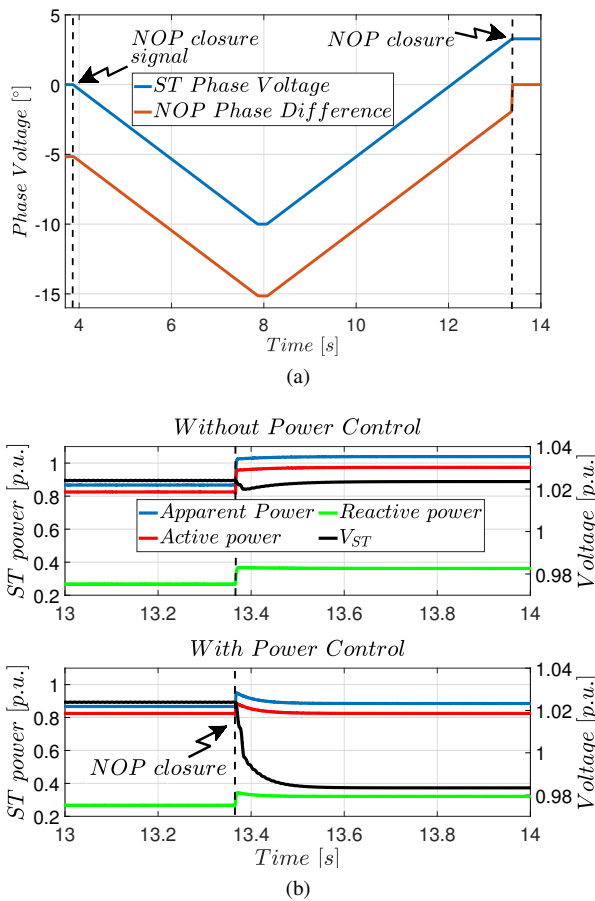
Fig. 7. (a) ST voltage phase angle and voltage phase difference at NOP extremities, respectively in blue and red line; (b) ST apparent, active and reactive power, and voltage respectively in blue, red, green, and black lines, in case of NOP closure for CT-fed LV grid undervoltage without and with power control.

(ca. 60 ms). The ST power control loop adjusts the voltage magnitude (black line in Fig.7b), reducing it from 1.025 pu to 0.983 pu. Despite the lower voltage quality, this reduction is temporary and it lasts only until receiving the NOP effective closure signal (i.e. few minutes). It is worth to note that the power variation, which corresponds to the NOP closure, occurs around 13.35 s, i.e. almost 10 s after the NOP signal. This is due to the 5° initial phase difference between the NOP terminals, that forces the phase variation algorithm to perform almost all the ramp signal before meeting the closure requirement of $-2° < \Delta\theta_{\mathrm{NOP}} < 2°$. This condition has been chosen, to examine a worst case scenario, where the whole angle ramp is needed to meet the NOP closure requirements. As can be seen from Fig.8, when the NOP closes, the reactive power increases, as illustrated from green line. The detection sensed by ST through (5) occurs 15 ms later.

To understand practically the impact of the filter time constant τ_{LPF} on the NOP closure detection, Fig.9 shows the response of the NOP closure detection for different time constant τ_{LPF}. As can be noted, a larger filter (e.g., $\tau_{LPF} = 0.2$ s) leads to a delayed detection, halting the angle with more than 60 ms delay with respect to the chosen value of $\tau_{LPF} = 0.05$ s.
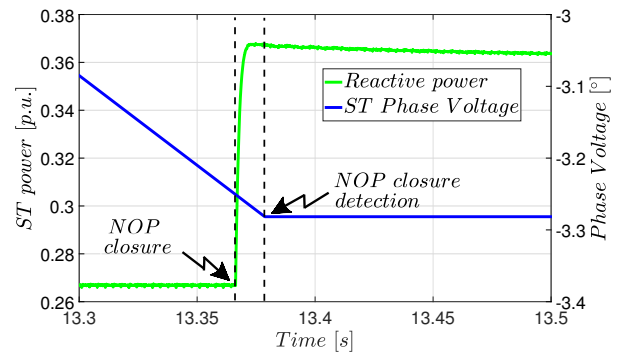

Fig. 8. Magnification of ST phase voltage, in blue line, and reactive power, in green line, during NOP closure.

B. DG Power Reduction During Closure Procedure

An issue that can be encountered during the closure procedure is a fast power change in the ST grid, due to a load disconnection, or the fast power variation from the DG, such as photovoltaic plants. In test case B, the same initial conditions as test case A are represented, i.e. $V_{\mathrm{CT}} = 0.95$ pu and $\theta_{\mathrm{CT}} = 5°$, while a sudden and unexpected power reduction of DG, corresponding to half of its delivering power, occurs immediately after that the ST receives the NOP signal. The first related problem is that the active power loop is already enabled, thus the ST does not change its power output to compensate the DG power reduction, but it keeps it at the value prior the NOP signal, as can be seen from black line of Fig.10. The robustness of the strategy is highlighted by the fact that the closure procedure is not interrupted because of the loss of generation, since this affects mainly active power, while the NOP closure detection is sensed through reactive power.

C. Synchronization in ideal conditions

In some cases, it may occur that the ST and the conventional transformer have the same voltage magnitude and angle (i.e, $V_{\mathrm{CT}} = 1.025$ pu and $\theta_{\mathrm{CT}} = 0°$). This case represents the optimal condition for synchronization, because no power increase or decrease is seen by the ST. Actually, the real ideal case is when the voltage magnitude and angle match at the two sides of the NOP. Nevertheless, the angle variation within a low voltage distribution grid is relatively small and sufficiently
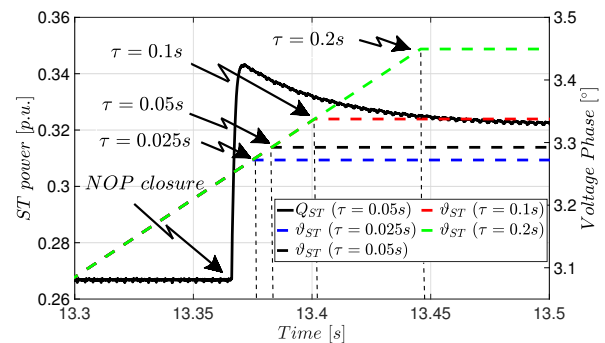

Fig. 9. ST reactive power (black line) and phase voltage for different τ_{LPF}.
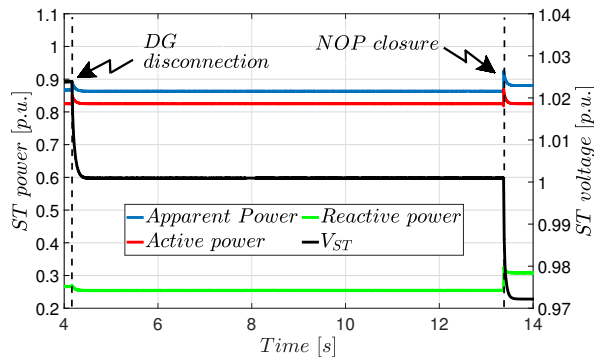
Fig. 10. ST apparent, active and reactive power, and voltage respectively in blue, red, green, and black lines in case of NOP closure for undervoltage of conventional transformer-fed LV grid and DG power reduction during closure procedure.

within the safety range of the NOP closure. For this reason, the same voltage magnitude and angle of the two transformers can be assumed as ideal conditions. In this situation the NOP closure could be achieved with no strategy implemented in ST, but because of the low bandwidth communication between NOP and ST, the synchronization strategy has to be initialized in any case. However, with respect to the previous cases, the closure detection cannot sense the reactive power change induced by the NOP closure, but only the one generated by phase variation. For this reason the reactive power threshold for detecting the NOP closure in (5) has to be carefully selected to recognize such condition. As can be seen in Fig.11, the chosen value of 0.02 pu is sufficient to recognize the NOP closure in around 200 ms.

D. Grid parameter variation analysis

The proposed strategy has been finally validated through several simulations under different grid parameters, i.e. DG generation and conventional transformer voltage. The NOP closure detection time has been measured and reported in Table V. It is worth to note that different load conditions do not affect significantly the time response of the strategy, which is very fast (less than $40ms$). Only the ideal conditions of the grid (i.e., both ST and conventional transformer with the same voltage angle) can really slow down the NOP closure detection, as has observed through test-case C. In this case the detection can reach up to $380ms$, and thus decrease the method performance. However, it must be remembered that an ideal condition does not imply any in-rush current flow during the NOP closure. Thus, the impact on the ST and local loads is minimal, and a longer detection does not represent an important issue.

VI. EXPERIMENTAL VALIDATION BY MEANS OF PHIL

The experimental verification of the ST synchronization strategy has been performed with the PHIL system shown in Fig.12. The hardware under test is the LV converter of the ST, the RTDS is the employed digital real time simulator, and the power amplifier is a Spitzenberger 3-phase PAS 15000 linear power amplifier. The PHIL evaluation is performed by

TABLE V
DETECTION TIME WITH PARAMETER VARIATION $[ms]$

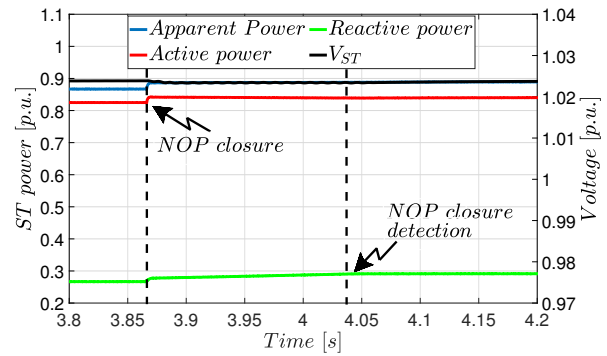|	DG power								
	90%			100%			110%		
θ_{CT}	V_{CT} $[pu]$								
	0.9	0.95	1	0.9	0.95	1	0.9	0.95	1
$-5°$	38	30	23	38	30	23	37	29	22
$0°$	**374**	**309**	250	**371**	**307**	249	**377**	**311**	253
$5°$	16	17	18	16	17	18	16	17	19

Fig. 11. ST apparent, active and reactive power, and voltage respectively in blue, red, green, and black lines, in case of NOP closure in ideal conditions.

means of a modified current-type ideal transformer method, that has been described in [29], and for this reason not repeated in this work. To validate the performance of the switching strategy, a sample LV network is simulated in RTDS, as in Fig.13. Between the ST hardware and the simulated grid, a current scale factor of 150 pu is introduced to address the different power scale between the simulated ST LV converter and the hardware one. As a consequence, 1 kW in hardware corresponds to 150 kW in the simulator.
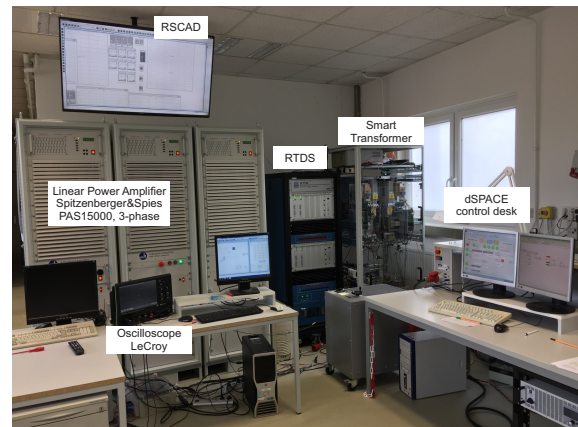

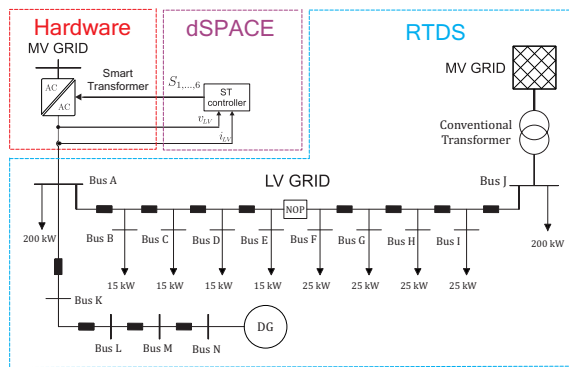Fig. 12. Power Hardware In the Loop experimental setup in the laboratory.

Fig. 13. Two-feeder radial distribution grid implemented in RSCAD (RTDS software) and PHIL description: Hardware of the PHIL setup (red frame), dSPACE interface (violet frame) and software of the PHIL setup (blue frame).
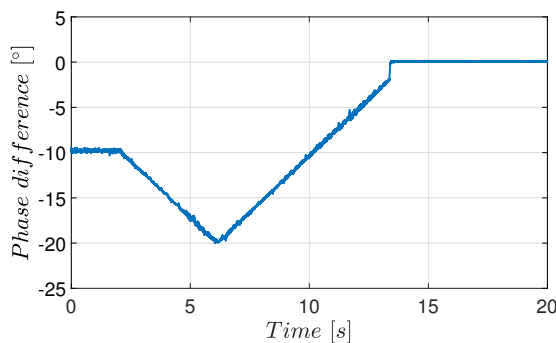

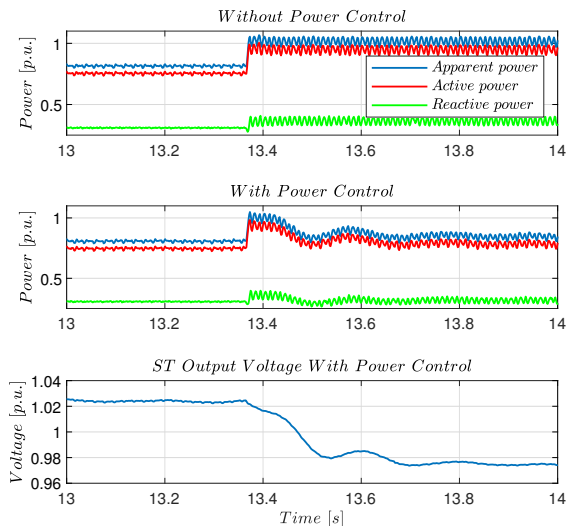Fig. 14. Phase voltage difference at NOP terminals.

Fig. 15. ST output active (red line), reactive (green line) and apparent power (blue line) without and with active power control, respectively, and ST output voltage with active power control.
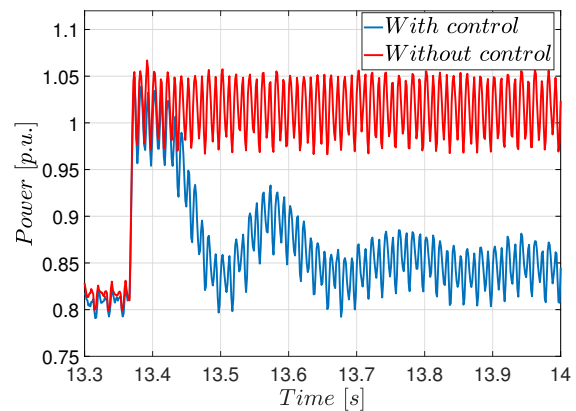

Fig. 16. Magnification of ST apparent power during NOP closure: with and without active power control, respectively in blue and red line.

A. Experimental Results

The test case A simulated in PLECS/Matlab software has been reproduced with PHIL evaluation to validate the proposed control strategy. Both the situations without and with power control have been tested. Fig.14 illustrates the voltage phase difference at NOP extremities. When the angle difference between the ST and the transformer grids is within $\pm 2°$, the NOP closes and thus the voltage phase difference rapidly becomes $0°$. The outcomes depicted in Fig.15 show a correspondence between simulation and experimental results. The first plot highlights that without power control the apparent power would settle at $1.04\,\mathrm{pu}$, that reflects what shown in the simulations and expected in the theory. If the power control is activated, the power surge is limited to few cycles, and the power is restored to the previous value. With respect to the simulations, the power controller shows an oscillating behavior with a frequency of 100 Hz, due to small unbalance in the current measurements in the RTDS. Nevertheless, no filter has been added at the output to avoid the slowing down of the dynamics. A better understanding of this transient can be achieved from its magnification during the NOP closure in Fig.16. The zoom shows how the power control limits the ST overload to three cycles (i.e., $60\,\mathrm{ms}$ in $50\,\mathrm{Hz}$ systems) that demonstrates that the proposed control is able to restore the ST apparent power below $1\,\mathrm{pu}$ dynamically.

VII. CONCLUSION

In this paper a synchronization strategy for ST meshed operations with a conventional transformer-fed grid is proposed, able to manage the power flow in-rush during the NOP switch closure. The introduced control strategy overcomes the physical distance and the lack of fast communication in the grid, relying only on the ST local measurements. The ST, working in voltage-forming mode during the synchronization, can adapt its voltage angle, within a certain range $[-10° \div 10°]$, to match the transformer-fed grid angle, and, thus, to close the NOP. The proposed synchronization procedure has proved to handle the active power in-rush from the ST, caused by possible difference in the two grid voltages. Employing an active power control, the ST can vary its voltage set-point, fixing its power injection to the value prior the NOP closure request. The impact of the proposed strategy on the ST-fed grid has been evaluated analytically and through simulation, and validated experimentally by means of Power-Hardware-In-Loop system. Results show a fast and safe management of the ST power during the synchronization transients.

REFERENCES

[1] D. L. Ransom, "Get in step with synchronization," *IEEE Trans. Ind. Appl.*, vol. 50, no. 6, pp. 4210–4215, Nov 2014.

[2] M. Liserre, G. Buticchi, M. Andresen, G. De Carne, L. F. Costa, and Z. Zou, "The smart transformer: Impact on the electric grid and technology challenges," *IEEE Ind. Electron. Mag.*, vol. 10, no. 2, pp. 46–58, June 2016.

[3] J. E. Huber and J. W. Kolar, "Applicability of solid-state transformers in today's and future distribution grids," *IEEE Trans. Smart Grid*, vol. 10, no. 1, pp. 317–326, Jan 2019.

[4] X. Yu, X. She, X. Zhou, and A. Q. Huang, "Power management for dc microgrid enabled by solid-state transformer," *IEEE Trans. Smart Grid*, vol. 5, no. 2, pp. 954–965, March 2014.

[5] L. Ferreira Costa, G. De Carne, G. Buticchi, and M. Liserre, "The smart transformer: A solid-state transformer tailored to provide ancillary services to the distribution grid," *IEEE Power Electron. Mag.*, vol. 4, no. 2, pp. 56–67, June 2017.

[6] T. M. L. Assis and G. N. Taranto, "Automatic reconnection from intentional islanding based on remote sensing of voltage and frequency signals," *IEEE Trans. Smart Grid*, vol. 3, no. 4, pp. 1877–1884, Dec 2012.

[7] J. M. Guerrero, J. C. Vasquez, J. Matas, L. G. de Vicuna, and M. Castilla, "Hierarchical control of droop-controlled ac and dc microgrids—a general approach toward standardization," *IEEE Trans. Ind. Electron.*, vol. 58, no. 1, pp. 158–172, Jan 2011.

[8] "Lv engine," 2018. [Online]. Available: https://www.spenergynetworks.co.uk/pages/lv_engine.aspx

[9] Y. A. I. Mohamed and A. A. Radwan, "Hierarchical control system for robust microgrid operation and seamless mode transfer in active distribution systems," *IEEE Trans. Smart Grid*, vol. 2, no. 2, pp. 352–362, 2011.

[10] L. G. Meegahapola, D. Robinson, A. P. Agalgaonkar, S. Perera, and P. Ciufo, "Microgrids of commercial buildings: Strategies to manage mode transfer from grid connected to islanded mode," *IEEE Trans. Sustain. Energy*, vol. 5, no. 4, pp. 1337–1347, 2014.

[11] M. Ganjian-Aboukheili, M. Shahabi, Q. Shafiee, and J. M. Guerrero, "Seamless transition of microgrids operation from grid-connected to islanded mode," *IEEE Trans. Smart Grid*, vol. 11, no. 3, pp. 2106–2114, 2020.

[12] M. Karimi-Ghartemani, "Universal integrated synchronization and control for single-phase dc/ac converters," *IEEE Trans. Power Electron.*, vol. 30, no. 3, pp. 1544–1557, 2015.

[13] X. Hou, Y. Sun, J. Lu, X. Zhang, L. H. Koh, M. Su, and J. M. Guerrero, "Distributed hierarchical control of ac microgrid operating in grid-connected, islanded and their transition modes," *IEEE Access*, vol. 6, pp. 77 388–77 401, 2018.

[14] T. L. Vandoorn, B. Meersman, J. D. M. De Kooning, and L. Vandevelde, "Transition from islanded to grid-connected mode of microgrids with voltage-based droop control," *IEEE Trans. Power Syst.*, vol. 28, no. 3, pp. 2545–2553, Aug 2013.

[15] A. Micallef, M. Apap, C. Spiteri-Staines, and J. M. Guerrero, "Single-phase microgrid with seamless transition capabilities between modes of operation," *IEEE Trans. Smart Grid*, vol. 6, no. 6, pp. 2736–2745, 2015.

[16] J. C. Vasquez, J. M. Guerrero, M. Savaghebi, J. Eloy-Garcia, and R. Teodorescu, "Modeling, analysis, and design of stationary-reference-frame droop-controlled parallel three-phase voltage source inverters," *IEEE Trans. Ind. Electron.*, vol. 60, no. 4, pp. 1271–1280, 2013.

[17] A. Vukojevic and S. Lukic, "Microgrid protection and control schemes for seamless transition to island and grid synchronization," *IEEE Trans. Smart Grid*, vol. 11, no. 4, pp. 2845–2855, 2020.

[18] J. Westman, R. Hadidi, J. C. Fox, J. Leonard, and A. Harrell, "Controller-hardware-in-the-loop testing of an iec 61850 goose based control for seamless transition of a microgrid between island and grid connected modes," *IEEE Trans. Ind. Appl.*, pp. 1–1, 2020.

[19] C. Sun, G. Joos, S. Q. Ali, J. N. Paquin, C. M. Rangel, F. A. Jajeh, I. Novickij, and F. Bouffard, "Design and real-time implementation of a centralized microgrid control system with rule-based dispatch and seamless transition function," *IEEE Trans. Ind. Appl.*, vol. 56, no. 3, pp. 3168–3177, 2020.

[20] G. G. Talapur, H. M. Suryawanshi, L. Xu, and A. B. Shitole, "A reliable microgrid with seamless transition between grid connected and islanded mode for residential community with enhanced power quality," *IEEE Trans. Ind. Appl.*, vol. 54, no. 5, pp. 5246–5255, 2018.

[21] J. Kwon, S. Yoon, and S. Choi, "Indirect current control for seamless transfer of three-phase utility interactive inverters," *IEEE Trans. Power Electron.*, vol. 27, no. 2, pp. 773–781, 2012.

[22] M. N. Arafat, S. Palle, Y. Sozer, and I. Husain, "Transition control strategy between standalone and grid-connected operations of voltage-source inverters," *IEEE Trans. Ind. Appl.*, vol. 48, no. 5, pp. 1516–1525, 2012.

[23] J. Chen, S. Hou, and J. Chen, "Seamless mode transfer control for master-slave microgrid," *IET Power Electron.*, vol. 12, no. 12, pp. 3158–3165, 2019.

[24] M. Ashabani, F. D. Freijedo, S. Golestan, and J. M. Guerrero, "Inducverters: Pll-less converters with auto-synchronization and emulated inertia capability," *IEEE Trans. Smart Grid*, vol. 7, no. 3, pp. 1660–1674, 2016.

[25] J. Wang, N. C. P. Chang, X. Feng, and A. Monti, "Design of a generalized control algorithm for parallel inverters for smooth microgrid transition operation," *IEEE Trans. Ind. Electron.*, vol. 62, no. 8, pp. 4900–4914, 2015.

[26] D. S. Ochs, B. Mirafzal, and P. Sotoodeh, "A method of seamless transitions between grid-tied and stand-alone modes of operation for utility-interactive three-phase inverters," *IEEE Trans. Ind. Appl.*, vol. 50, no. 3, pp. 1934–1941, 2014.

[27] X. She, A. Q. Huang, and R. Burgos, "Review of solid-state transformer technologies and their application in power distribution systems," *IEEE Trans. Emerg. Sel. Topics Power Electron.*, vol. 1, no. 3, pp. 186–198, Sep. 2013.

[28] C. Kumar and M. Liserre, "Operation and control of smart transformer for improving performance of medium voltage power distribution system," in *2015 IEEE 6th International Symposium on Power Electronics for Distributed Generation Systems (PEDG)*, June 2015, pp. 1–6.

[29] G. De Carne, G. Buticchi, and M. Liserre, "Current-type power hardware in the loop (phil) evaluation for smart transformer application," in *2018 IEEE International Conference on Industrial Electronics for Sustainable Energy Systems (IESES)*, Jan 2018, pp. 529–533.

Stefano Giacomuzzi received the B.Sc. degree in Energy Engineering and M.Sc. degree in Electrical Engineering from the University of Padova, Padua, Italy, in 2013 and 2016, respectively. In 2016 he received a research grant for the research project "AC Electric Energy Hub" at the Department of Industrial Engineering, University of Padova. He is currently a Ph.D. candidate at the same department. In 2019 he was a visiting Ph.D. student at the Chair of Power Electronics, Kiel, Germany.

His research interests include power electronics circuits and control systems for renewable energy sources, microgrids management and smart transformers applications.

Giovanni De Carne (S'14, M'17) received the B.Sc. and M.Sc. degrees in electrical engineering from the Polytechnic University of Bari, Italy, in 2011 and 2013, respectively, and the Ph.D. degree from the Chair of Power Electronics, Kiel University, Germany, in 2018. He was post-doctoral fellow at Kiel University working on HVdc control and services until 2019. He is currently the Head of the "Real Time System Integration" Group and of the "Power Hardware In the Loop Lab" at the Institute for Technical Physics at the Karlsruhe Institute of Technology.

In 2020, he has been awarded with the Helmholtz "Young Investigator Group" for the project "Hybrid Networks: a multi-modal design for the future energy system".

He has authored/coauthored more than 60 peer-reviewed scientific papers. His research interests include power electronics transformers, real time modelling, and power hardware in the loop. He is an Associate Editor of the IEEE Industrial Electronics Magazine and Springer Journal Electrical Engineering.

Sante Pugliese (M'18) received the M.Sc. degree in automation engineering and the Ph.D. degree in electrical and information engineering from the Politecnico di Bari, Bari, Italy, in 2013 and 2018, respectively.

In 2017, he was a Visiting Scholar with the Chair of Power Electronics, Kiel, Germany, where he is currently a Post-Doctoral Researcher. His research interests include power converters and control techniques for distributed power generation systems based on renewable energies.

Giuseppe Buja (M'75-SM'84-F'95-LF'13) received the Laurea degree (Hons.) in power electronics engineering from the University of Padova, Padova, Italy.

He is currently an Honorary Research Scientist with the University of Padova. He has carried out pioneering research works in power and industrial electronics, originating the modulating-wave distortion, optimum modulation for pulse-width modulation inverters, initiating the application of digital signal processors to the control systems of power electronics converters, and conceiving advanced techniques for the control of electric drives. His research interests include automotive electrification, including wireless charging of electric vehicles and grid-integration of renewable energy sources.

Dr. Buja is a member of the International Conference Steering/Technical Committees and the Scientific Journal Editorial Boards. He is also a Senior Member of the Administrative Committee, IES. He received the IEEE Industrial Electronics Society (IES) Eugene Mittelmann Achievement Award in recognition of the outstanding technical contributions in industrial electronics, and the 2016 Best Paper Award from the IEEE TRANSACTIONS ON INDUSTRIAL ELECTRONICS. He served the IEEE in several capacities, including the General Chairman of the 20th Annual Conference of IES (IECON, in 1994). He served as an Associate Editor for the IEEE TRANSACTIONS ON INDUSTRIAL ELECTRONICS.

Marco Liserre (S'00-M'02-SM'07-F'13) received the MSc and PhD degree in Electrical Engineering from the Bari Polytechnic, respectively in 1998 and 2002. He has been Associate Professor at Bari Polytechnic and from 2012 Professor in reliable power electronics at Aalborg University (Denmark). From 2013 he is Full Professor and he holds the Chair of Power Electronics at Kiel University (Germany). He has published 500 technical papers (1/3 of them in international peer-reviewed journals) and a book. These works have received more than 35000 citations. Marco Liserre is listed in ISI Thomson report "The world's most influential scientific minds" from 2014.

He has been awarded with an ERC Consolidator Grant for the project "The Highly Efficient And Reliable smart Transformer (HEART), a new Heart for the Electric Distribution System".

He is member of IAS, PELS, PES and IES. He has been serving all these societies in different capacities. He has received the IES 2009 Early Career Award, the IES 2011 Anthony J. Hornfeck Service Award, the 2014 Dr. Bimal Bose Energy Systems Award, the 2011 Industrial Electronics Magazine best paper award and the Third Prize paper award by the Industrial Power Converter Committee at ECCE 2012, 2012, 2017 IEEE PELS Sustainable Energy Systems Technical Achievement Award and the 2018 IEEE-IES Mittelmann Achievement Award.

Ali Kazerooni received received his Ph.D. degree from University of Manchester. He is currently a chartered engineer with SP Energy Networks, Future Networks team, as technical lead and project manager for complex projects. He previously was power systems team lead with WSP where he led several innovation projects with UK Distribution Network Operators. He has been focusing on developments and applications of power electronic solutions and their control systems for grid applications. That includes the concept development and initial feasibility studies to implementation and live demonstrations.

Dr. Kazerooni is now heavily involved in delivery of LV Engine project which is a flagship smart grid project aiming to trial smart transformers in different network operation arrangements. He has been author and co-author of several technical papers presented in conferences and international journals.